JOURNAL OF AIRCRAFT
Vol. 36, No. 3, May–June 1999

Freestream Disturbance Effects on an Airfoil Pitching at Constant Rate

Jerry M. Chen* and Chih-Chung Choa†
National Chung-Hsing University, Taichung 402, Taiwan, Republic of China

Effects of freestream disturbances on the dynamic stall process of an NACA 0012 airfoil undergoing ramp-type pitching motion from 0–30 deg were studied using measurements of unsteady surface pressures. A thin circular cylinder was located upstream of the test airfoil and was offset vertically between −0.133 and 0.133 chord lengths with respect to the airfoil pitching axis to provide the freestream disturbances. The measurements were carried out at a constant chord Reynolds number of 8×10^4 for a relatively low reduced pitch-rate range $k = 0.01$–0.04. As compared with the undisturbed flow case, the imposed freestream disturbances were able to produce a significant increase in absolute magnitude of the peak suction pressure near the leading edge, resulting in a noticeable phase delay in stall process. The growth of the leading-edge suction peak caused by insertion of the upstream rod was found to be sensitive to its vertical offset position. Nevertheless, the pressure variation caused by the freestream disturbances was appreciable only in the forward 20% chord from the leading edge, bringing a lower effect on the airfoil lift and momentum coefficients.

Nomenclature

Cl = sectional lift coefficient
$Cl_{\max}$ = maximum sectional lift coefficient
Cm = sectional pitching-moment coefficient
C_p = pressure coefficient, $(P - P_\infty)/(\rho U_\infty^2/2)$
c = airfoil chord
k = reduced pitch rate, $\dot{\alpha}c/2U_\infty$
P = pressure at a point on the airfoil surface
P_∞ = freestream static pressure
Re = Reynolds number based on chord
T = airfoil pitch-up time
t = time
U_∞ = undisturbed freestream velocity
u, v = streamwise and transverse components of the time-mean velocity
u', v' = rms of the streamwise and transverse components of the velocity fluctuations
X_R = horizontal distance from the rod, see Fig. 1
x = axial distance from leading edge
Y_R = vertical offset distance of the rod, see Fig. 1
y = transverse coordinate fixed on the rod center
α = angle of attack
$\dot{\alpha}$ = angular velocity of pitching
ρ = fluid density
τ = nondimensional time, t/T

Introduction

IT is generally recognized that rapidly pitching an airfoil to high angles of attack can lead to the generation of much greater lift (albeit transient), compared with its static counterparts, and that stall is delayed until an angle of attack much higher than in the static cases is encountered. This phenomenon has been observed to be associated with the formation and shedding of a large-scale vortex known as the dynamic stall vortex (DSV) that develops from the leading-edge region of the airfoil.[1–3] Dynamic stall is of importance in a variety of rotational machinery, such as helicopter rotors, compressors, and wind turbines. Furthermore, there has been some interest in exploiting dynamic vortex lift by pitching an airfoil in applications related to enhancement of the maneuverability and the agility of fixed wing aircraft; although sustained integrated lift has been shown to be less than the static $Cl_{\max}$ if dynamic vortices are formed.[4]

Experimental studies on airfoil dynamic stall have so far generally been performed in smooth freestream across a wide range of parameters including airfoil shape; Mach number; Reynolds number; and the form, rate, and amplitude of the forcing motion.[5–14] The influence of freestream disturbances has received little attention. However, in practical applications, the freestream environment encountered by an airfoil is often disturbed by other upstream components of the aircraft. Such a situation may occur for aircraft with the configurations of wing–body, canard–wing, wing–tail, and other combinations. For a static airfoil at low chord Reynolds numbers of typically 10^4–10^6, it is known that the boundary layers developed on the airfoil surfaces are sensitive to the freestream environment. The boundary layers in this low-Reynolds-number regime are often characterized by laminar separation from the surface of the airfoil and turbulent reattachment to the surface some distance downstream.[15] The region underneath the separated flow, between the points of separation and reattachment, is referred to as a laminar separation bubble or simply as a bubble. If a leading-edge bubble is present, the usual characteristic that appears in the lift curve is a plateau for a small angle-of-attack range before resuming the increase in Cl with increasing angle.[16,17] Although for some airfoil sections, such as NACA 0012 and NACA 0015, their static lift variations were shown to be rather gradual continuous, indicating trailing-edge stall, during dynamic tests the airfoils might experience a plateau in lift curves, signifying possible leading-edge bubbles. In any event, an increase in turbulence levels may alter the locations on the surface and the incidences of the airfoil at which the separation and reattachment take place, and consequently change the stalling behavior of the airfoil.[18,19] Conger and Ramaprian,[20] who pitched an NACA 0015 airfoil in a water channel with a relatively higher freestream turbulence level (0.8–1.0%), found the magnitudes of pressure and lift force measured to be much larger than those obtained in earlier experiments performed for similar Reynolds numbers and pitch rates. They suspected that the high freestream turbulence could promote early laminar-turbulent transition in the boundary layer, and, hence, suppress the separation region on the suction surface of the airfoil, resulting in a flow behavior comparable to that at much higher Reynolds numbers. Laneville and Vittecoq,[21] in a study of wind turbines, also discovered that freestream turbulence intensity could have a large effect on the development of the dynamic stall of low-Reynolds-number airfoils.

Received March 1, 1998; revision received Nov. 2, 1998; accepted for publication Nov. 17, 1998.

*Associate Professor, Department of Mechanical Engineering. Member AIAA.
†Graduate Assistant, Department of Mechanical Engineering.

Although the aforementioned studies seem to have provided a qualitative view of the role of freestream disturbances in the dynamic stall process developed on a rapidly pitching airfoil, quantitative effects of the disturbances remain unclear.

The present study is a continuation of our previous investigation[22] that involved measurements of unsteady surface pressures on a pitching airfoil of an NACA 0012 profile for various reduced pitch rates and Reynolds numbers in smooth flow. The work presented here is focused on the influence of freestream disturbances on the unsteady aerodynamic and dynamic stall characteristics of the airfoil undergoing ramp-type pitching motion from zero incidence to an angle of attack of 30 deg. To produce the freestream disturbances, a thin rod of 5 mm diameter was immersed at a certain distance upstream of the pitching airfoil. The influence of disturbances was examined by measuring the chordwise surface pressures on the airfoil. The pressures were spatially integrated to obtain the time-varying sectional lift force and pitching moment of the airfoil. The measurements were carried out for different vertical positions of the rod with respect to the pitching axis of the airfoil. Another experimental parameter was the reduced pitch rate that was varied in a relatively low range ($0.01 \leq k \leq 0.04$) in the present study. As will be shown later, even in this low range of pitch rate, the maximum coefficients of lift can reach more than double the static $Cl_{\max}$.

Experimental Setup

Figure 1 shows the schematic of the experimental arrangement of a pitching airfoil subjected to freestream disturbances. The experiments were conducted in an open-type wind tunnel with a test section of 0.305×0.305 m and 1.100 m in length. The undisturbed flow into the test section had a turbulence level lower than 0.5%. The airfoil of NACA 0012 with a chord of $c = 0.150$ m and an aspect ratio of 2.02 was horizontally mounted at the midheight of the test section, leaving a 1-mm gap between the wing and the wall at each side of the tunnel. A digitally controlled servomotor was employed to pitch the airfoil about its quarterchord. An optical encoder was coupled to the motor shaft to signify the transient angle of incidence of the airfoil. The signal from the encoder was also used for the angular reference of measurements. The airfoil was initially held at zero incidence, then pitched at constant angular velocity $\dot{\alpha}$ to 30 deg, and held there. This yields a ramp motion that begins at a nondimensional time $\tau = t/T$ of 0 and ends at $\tau = 1$, where T is the pitch-up period. Repeated tests showed that the uncertainty of the angular position of the ramp airfoil was within ± 0.1 deg.

The freestream disturbances incident upon the pitching airfoil were generated using a circular rod of 5 mm diam. The rod was spanned across the test section and was placed upstream of the test airfoil. Such a technique to generate freestream disturbances is similar to that employed by Kiya and Sasaki.[23] Throughout the experiments, the freestream velocity and the horizontal distance between the upstream rod and the pitching axis of the airfoil were kept constant, while the vertical offset distance was varied. The freestream velocity was $U_\infty = 8.0$ m/s, corresponding to a Reynolds number of 8.0×10^4, based on the airfoil chord. The horizontal distance between the rod and the quarterchord was $1.2c$. The rod was offset vertically in the range $-0.133 \leq Y_R/c \leq 0.133$.

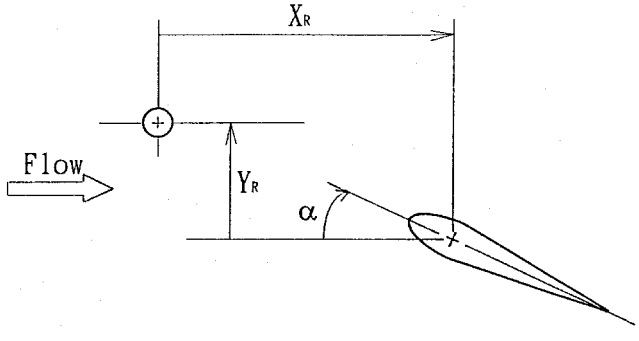

Fig. 1 Geometric parameters of the experimental arrangement.

The fluctuating and time-mean velocities in the wake of the rod were measured using an anemometry system (TSI IFA 100) in conjunction with an X-film probe. The wake surveys were made in the absence of the airfoil model, and the measurements were performed in the centerline plane of the test section for several streamwise locations. For each streamwise location, the probe was traversed for at least 55 vertical stations, covering $-0.27 \leq y/c \leq 0.27$, equidistant from the rod center. The unsteady pressures on the surface of the pitching airfoil were measured by differential pressure transducers (ScanCo PDCR23D). There were 23 pressure ports instrumented along the midspan of the airfoil model. Twelve of the pressure ports were located at 0.5, 2.5, 7.5, 12.5, 20, 30, 40, 50, 60, 70, 80, and 90% chord on the upper surface. The remaining 11 ports were at 1, 5, 10, 15, 25, 35, 45, 55, 65, 75, and 85% chord on the lower surface. Each of the pressure ports was connected with a 0.30 m length of 1.59-mm-i.d. Teflon® tubing to the transducer. The pressure transducer alone had a natural frequency higher than 1.8 kHz that was well above the dynamic range of interest. However, the connection of the tubing to the transducer could reduce the frequency response. An extensive calibration method similar to those employed by Batill and Nebres[24] and Rennie and Jumper[25] was used to examine the amplitude and phase distortion of the pressure signal owing to the tubing. The amplitude response was found to be flat (less than 4% deviation) up to a frequency of ~30 Hz, and the phase lag caused by the tubing had a linear variation with frequency up to ~45 Hz. As compared with the stall sharpness of the dynamic lift curves acquired, such an arrangement for pressure measurements suffices for the present investigation.

The signals from the anemometers and the pressure transducer as well as the encoder of the servomotor were acquired by a four-channel transient recorder (ADAM ADC 0512). In making unsteady pressure measurements, two transducers were used during a single dynamic experimental run, one measuring the pressure port of interest, the other serving to verify the repeatability of the dynamic signal. Moreover, in the unsteady measurements, it was necessary to use a reference phase to trigger the data recording system. This trigger pulse was provided by the starting signal of the servomotor. The ensemble-average method was employed to obtain the unsteady pressure distribution on the pitching airfoil. Four independent realizations (multiple pitches) were averaged for unsteady pressure measurements. This number of realizations was to make a compromise between overall measurement time and accuracy. The pressure coefficient C_p was calculated in reference to the freestream static pressure. The rms error in C_p was 0.06 for a typical ensemble-average data set measured at the pressure port $x/c = 0.5\%$, which had the largest variation of pressure coefficient with time as compared with other pressure ports. The pressure data were spatially integrated to obtain the sectional lift and moment of the airfoil. The uncertainties (because of random errors) in lift coefficient Cl and moment coefficient Cm were approximately ± 5 and ± 6% of the maximum/minimum values measured, respectively. The unsteady pressure measurements were performed for reduced pitch rates k ($=\dot{\alpha}c/2U_\infty$) of 0.01, 0.02, and 0.04. In the worst case, the blockage ratio caused by the tunnel walls was about 25%. For the data described here, no blockage corrections were made because these data were collected mainly for comparing the relative performance of the airfoil with and without the freestream disturbances. Nevertheless, it may be worth making a calculation as to what one may expect the blockage to do to the data. The static, wind-tunnel wall blockage correction to the lift coefficient was calculated, following a method based on Ref. 26 to be less than 14% for $\alpha = 15$ deg and 19% for $\alpha = 25$ deg. The unsteady blockage correction would be smaller than the static value. In the present investigation, the use of a rather low-aspect ratio airfoil may also deserve some comments. To check for sidewall effects, two additional pressure points were located at $0.4c$ on either side of the midspan at a chordwise position of $0.2c$ from the leading edge. For all pitch rates tested in the experiments, the maximum variation of C_p between the three spanwise locations at $x/c = 0.2$ was found to be small (less than ± 4.5%), up to the interception of the dynamic stall that occurred before the airfoil was suddenly held at $\alpha = 30$ deg in most of the cases presented

here. Furthermore, the lifting-line theory may be used to calculate the sectional lift at each spanwise station of a steady wing in the absence of the tunnel walls. As described in Ref. 27, knowledge of the steady two-dimensional airfoil lift-slope is required for the calculation. With a typical lift-curve slope value of 1.8π for the airfoil employed in the present experiments, the static Cl calculated at $0.4c$ either side of the midspan was 8% less than at the midspan. For a dynamic airfoil, this difference would be much smaller.[28] Hence, the sidewall interference may not significantly affect the results of the present investigation, at least when the flow is attached.

Results and Discussion

Nature of the Disturbances

The wake of a circular cylinder could develop into turbulence for Reynolds numbers greater than 2×10^2, and the region of transition to turbulence would move toward the cylinder with increasing Reynolds number.[29] For the present experiments, the thin circular rod of 5 mm diam that was located upstream of the pitching airfoil to generate freestream turbulence gave a Reynolds number of 2.7×10^3, based on the rod diameter. Wake surveys were made to determine the character of the generated freestream disturbances. The wake velocities were measured along several survey line positions covering the entire region at which the test airfoil was horizontally held, i.e., from the leading edge ($X_R/c = 0.92$) to the trailing edge ($X_R/c = 1.92$). Figure 2 shows the time-mean streamwise velocity profiles of the half-wake and the accompanying turbulence intensities in the streamwise and transverse directions. For the data presented in this figure, the uncertainties in u, u', and v' are approximately ± 3.6, ± 5, and $\pm 6\%$ of the value of the freestream velocity, respectively. It can be seen that the centerline velocity defect decays with the downstream distance from $0.19U_\infty$ at $X_R/c = 0.92$ to $0.13U_\infty$ at $X_R/c = 1.92$. The semiwake width, which is defined as the width of the wake where the total mean velocity defect is one-half of the velocity defect at the wake center, maintains at a nearly constant value $0.04c$ between $X_R/c = 0.92$ and 1.25, and then increases to about $0.07c$ at more downstream locations $X_R/c = 1.58$ and 1.92. The momentum thickness of semiwake also displays a similar trend that is a change of $0.0067c$ at $X_R/c = 0.92$ and 1.25 to about $0.0105c$ at $X_R/c = 1.58$ and 1.92. The turbulence intensity profiles suggest that the total introduced freestream turbulence within the semiwake width is more than 6% for the forward two streamwise locations, and slightly reduces to ~5% for the two farther downstream locations. The profiles also indicate that the freestream turbulence is localized within a transverse distance of about $0.15c$ from the centerline of the wake. Moreover, the frequency spectra of the measured reference turbulence exhibited no definite peaks associated with the rod's vortex shedding frequencies that were expected to be around 336 Hz. This signifies that the organized vortices shed from the rod, that would have introduced the dependence of phase difference into the flow during the pitching process, had decayed to a great extent before they arrived in the region where the test airfoil was placed.

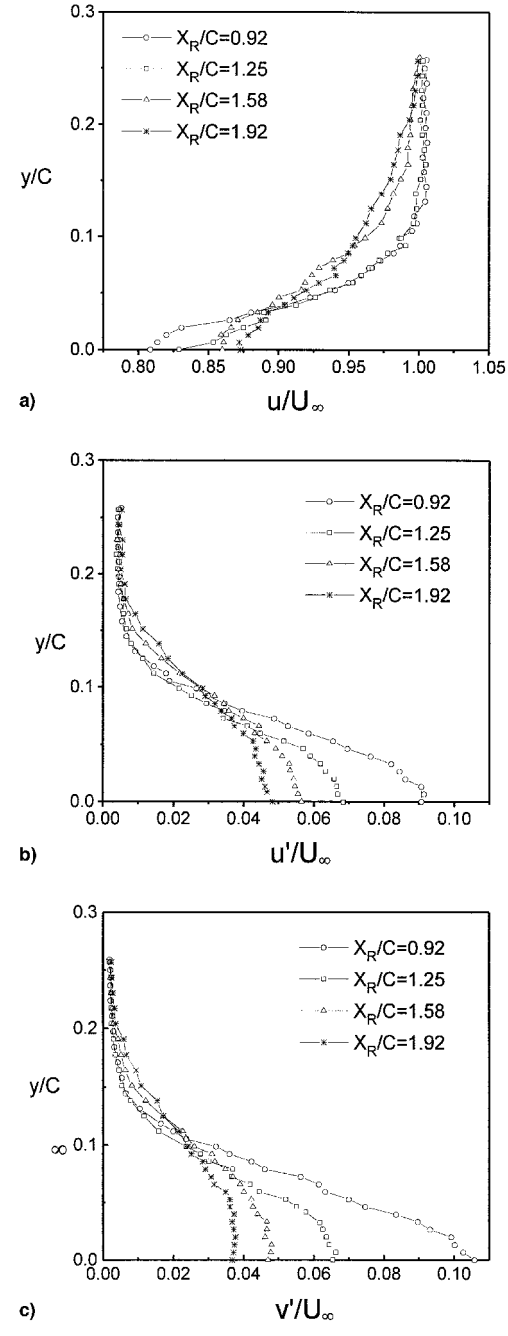

Fig. 2 Velocity profiles and turbulence intensity distributions measured behind the rod: a) time-mean velocity, b) rms of fluctuating streamwise velocity, and c) rms of fluctuating transverse velocity.

Static Airfoil

Prior to the measurements on the pitching airfoil, the pressure distributions and the corresponding lift forces were examined for the airfoil fixed at an angle of attack. The static tests were taken for angles of attack ranging from 0–16 deg under disturbed or undisturbed conditions, and all pressure and lift coefficients were nondimensionalized with the undisturbed freestream velocity. Figure 3 presents the comparison of the lift curves obtained for offset values Y_R/c between -0.133 and 0.133 with the undisturbed case. At lower angles of attack ($\alpha < 10$ deg), there appears to be no discernible change in the sectional lift-curve slope associated with the offset of freestream disturbances, except for $Y_R/c = 0$. The airfoil for $Y_R/c = 0$ that experienced a reduction in lift coefficient was encountering a lower effective freestream velocity in the wake. At around $\alpha = 10$ deg, stall occurs for the undisturbed airfoil and for the case of positive offset $Y_R/c = 0.133$. However, the imposed disturbances at $Y_R/c = 0$ and -0.133 are effective in extending the lift curve, increasing the maximum Cl to 1.05 and 1.03, and delaying the stall to $\alpha = 14$ and

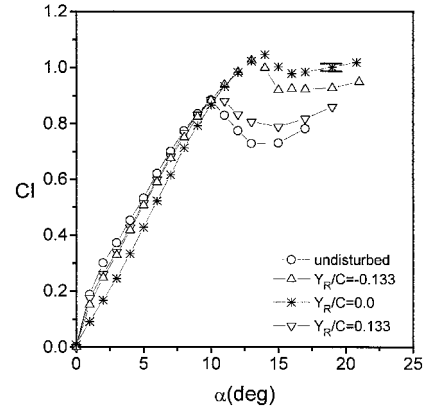

Fig. 3 Sectional lift curves of the static airfoil for disturbed and undisturbed cases.

13 deg, respectively. This may be attributed to the fact that the high turbulence being introduced upstream of the stagnation point of the airfoil is instrumental in energizing the boundary layer and delaying separation locations to higher angles of attack.[18,19] This explanation is consistent with the pressure distributions shown in Fig. 4 for vertical offset of the rod. While the upper-surface pressure becomes a rather flat distribution at $\alpha = 11$ deg for the undisturbed and the positive offset cases, the leading-edge suction peak reaches a large value of about 4.0 in absolute magnitude of C_p for the airfoil with $Y_R/c = 0$ and -0.133. It should be noted that the wake trajectory behind the upstream rod at a positive offset position of $Y_R/c = 0.133$ would be deflected upward when it approached the leading edge of the airfoil at high angles of attack. In other words, the effective offset is shifted in a positive sense as the airfoil incidence is increased.[30] As a result, the disturbances at $Y_R/c = 0.133$ appear to have an insignificant influence on the pressure distribution and the lift curve. The influence of the disturbances at $Y_R/c = 0.133$ was also found to be negligible in the dynamic tests. Therefore, only the results of the disturbances at $Y_R/c = 0$ and -0.133 will be presented hereafter to compare with those of the undisturbed airfoil.

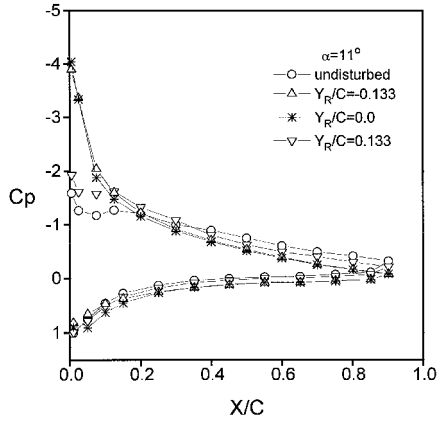

Fig. 4 Upper and lower surface pressure distributions of the static airfoil at α = 11 deg.

Pitching Airfoil

Figure 5 shows the pressure distributions on the suction surface of the pitching airfoil at different angles of attack. These results are presented for a lower pitch rate $k = 0.01$ and for the disturbed and undisturbed cases. The pressure distributions presented in Fig. 5 exhibit a leading-edge suction peak at $x/c = 0.005$ under either the disturbed or undisturbed circumstance. The absolute magnitude of the suction peak grows until the airfoil reaches an angle of attack ~1–2 deg higher than its corresponding static stall angle. The leading-edge suction peak has a much larger magnitude and occurs at a higher angle of attack for the disturbed cases, particularly for the disturbances at $Y_R/c = -0.133$. When the growth of the leading-edge pressure ends, there is sudden collapse of this peak. In the meantime, a secondary suction peak is observed near $x/c = 0.125$. The appearance of the secondary suction peak and the collapse of the leading-edge suction peak indicate that the boundary layer begins to detach from the airfoil, forming a free shear layer.[5,20] Note that the secondary suction peak observed in Fig. 5 is relatively broad compared to those of higher pitch rates ($0.05 \le k \le 0.2$) performed by Conger and Ramaprian[20] and Chen and Lee,[22] implying a rather weak structure of DSV developed at $k = 0.01$ (Ref. 11). As the angle of attack is further increased, the secondary suction peak slowly spreads out and moves downstream.

The observation of Fig. 5 suggests a significant variation of the leading-edge and secondary peaks with the freestream disturbances and their offset values. This variation appears more appreciable at the pressure ports in the forward 20% chord from the leading edge of the airfoil. At more downstream chordwise locations ($x/c \ge 0.3$),

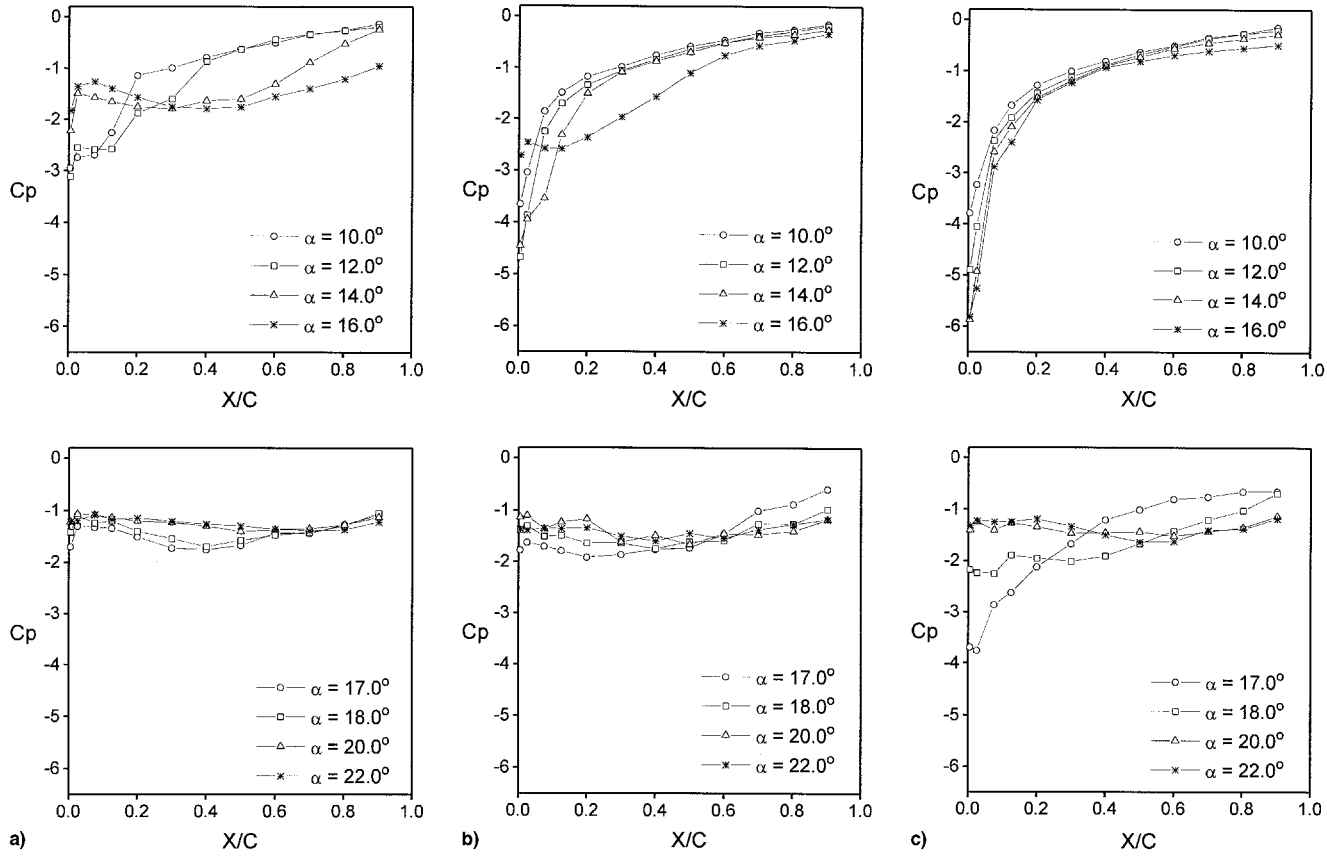

Fig. 5 Upper-surface pressure distributions of the airfoil pitching at k = 0.01: a) undisturbed case, b) disturbed at Y_R/c = 0, and c) disturbed at $Y_R/c = -0.133$.

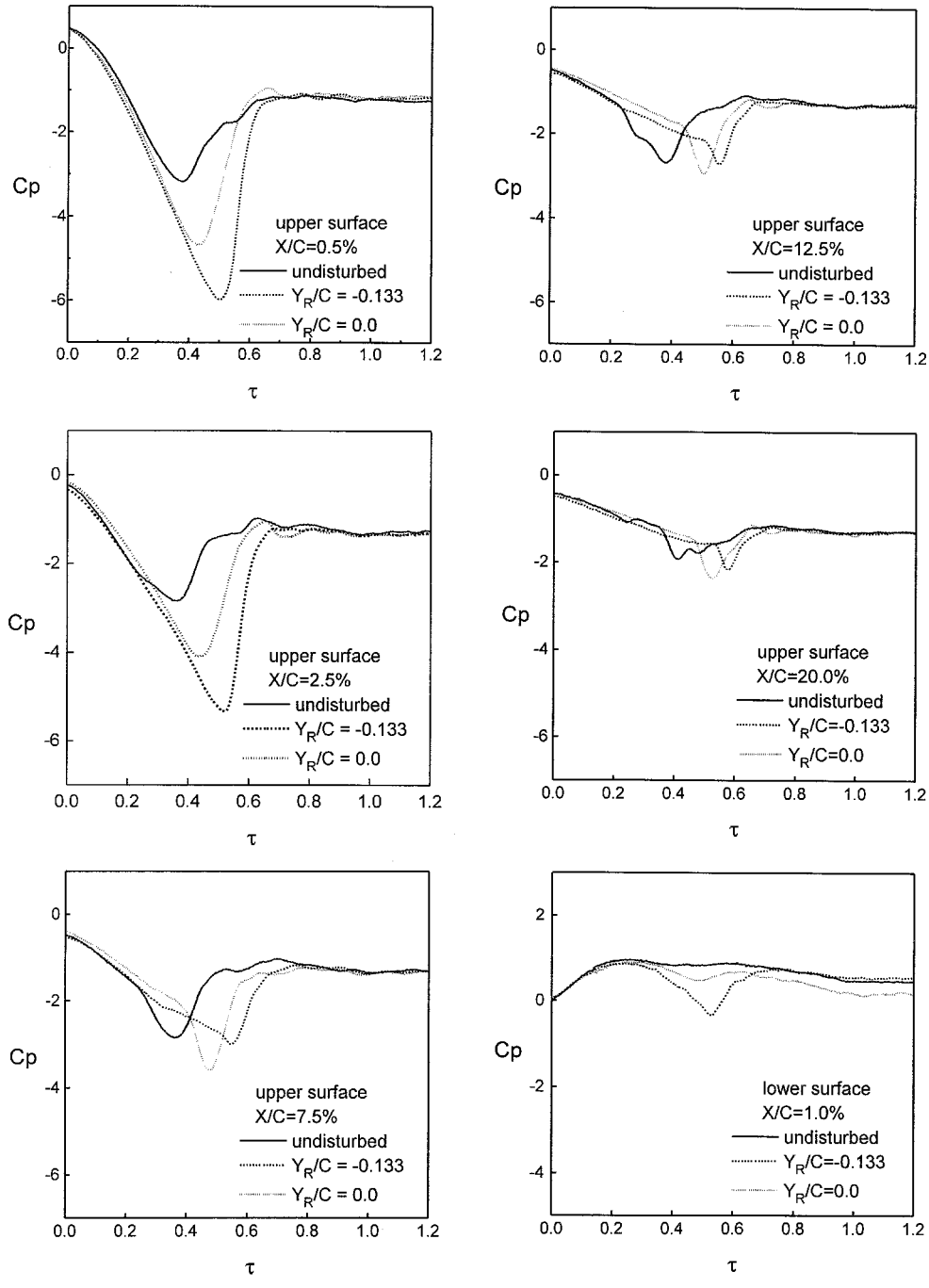

Fig. 6 Comparison of C_p time history for disturbed and undisturbed cases.

regardless of a phase lag, the difference in the maximum value of secondary suction between the disturbed and undisturbed cases was found to be within ± 0.1 in C_p. The effects of freestream disturbances may be revealed in a more apparent manner by comparing the time histories of C_p at several selected pressure ports shown in Fig. 6. These time histories include five upper-surface pressures at $x/c \leq 0.2$ and one lower-surface pressure at the nose ($x/c = 0.01$). These plots demonstrate that the upper-surface pressure responds smoothly to the change in pitch angle until a maximum suction (minimum C_p) is reached. Subsequently, the pressure rises, at a faster rate than it drops, to arrive at a nearly constant value. The variations of C_p time histories on the upper surface completed well before the airfoil motion stops at $\tau = 1.0$. It can be seen that a direct impingement of the disturbances ($Y_R/c = 0$) leads not only to an increase in magnitude of the maximum suction pressure, but also to a phase delay of the pitch angle at which the maximum is reached. As the disturbances are shifted to a negative offset ($Y_R/c = -0.133$), the magnitude of the maximum suction as well as the phase delay are further enlarged at the leading two pressure ports ($x/c = 0.005$ and 0.025). But the magnitude of maximum suction decreases with x/c more rapidly than that of the direct impingement. This indicates an earlier transition of the laminar boundary layer to turbulence, and thus, a shorter size of the separation region.[18,19] On the lower surface at $x/c = 0.01$, the pressure is influenced by the motion of stagnation point in response to the change in pitch angle. The pressure initially rises to reach a maximum at $\tau = 0.25$, and then it begins to decrease. The decrease in pressure seems to be associated with the variation of the leading-edge pressure on the upper surface. The most pronounced phase delay that occurs for the negative offset also prompts the lower-surface nose pressure to have a sharp drop to negative C_p.

The maximum values of suction pressure coefficient $-C_p$ are further plotted in Fig. 7 against the dimensionless time τ at which

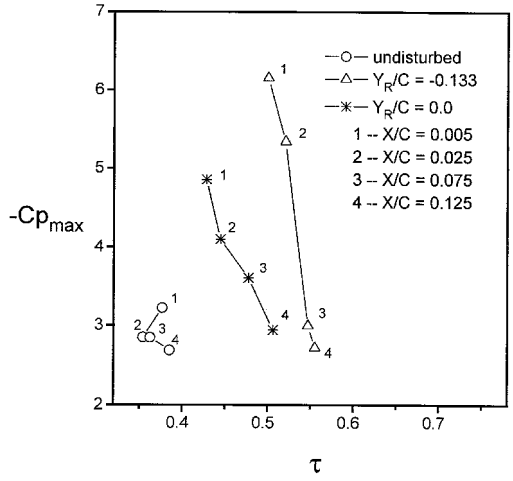

Fig. 7 C_p vs τ of maximum suction for the leading four pressure ports at k = 0.01.

the maximum occurs for the leading four upper-surface pressure locations, $x/c = 0.005$, 0.025, 0.075, and 0.0125. The dimensionless time that represents the pitch angle has an uncertainty of about ± 0.005. This plot summarizes the influence of the vertical offset of the disturbanceson the occurrenceof the maximum suction. As compared to the undisturbed case, which has a maximum leading-edge ($x/c = 0.005$) pressure of 3.5 in $-C_p$ occurring at $\alpha = 11.0$ deg, in the disturbed circumstance the maximum suction pressure coefficient at the leading edge is increased to 4.9 and 6.1 at $\alpha = 12.8$ and 15.0 deg for $Y_R/c = 0$ and -0.133, respectively. Although the introduction of freestream disturbances results in a significant change in pressures near the leading edge, the sectional lifts and quarter-chord moments appear to have a lower disturbance influence. This can be seen in Fig. 8 that shows the time histories of sectional lift and moment for the disturbed and undisturbed pitches at $k = 0.01$. Until the airfoil pitches up to its corresponding static stall angle, the lift curve behaves like the static airfoil. Thereafter, the lift continues to grow. For the undisturbed case, the maximum Cl of 1.50 is reached at $\alpha = 15.0$ deg. When the disturbances are imposed, the maximum Cl is slightly increased to 1.60 and 1.66 at $\alpha = 16.6$ and 18.0 deg for $Y_R/c = 0$ and -0.133, respectively. The time histories of Cm drop sharply at the time nearing the dynamic stall. The sharp drop of Cm also reflect a noticeable phase delay as a result of the imposed disturbances. In comparison with the undisturbed case, the drop is lagged by about 2.5 and 3.5 deg for $Y_R/c = 0$ and -0.133, respectively.

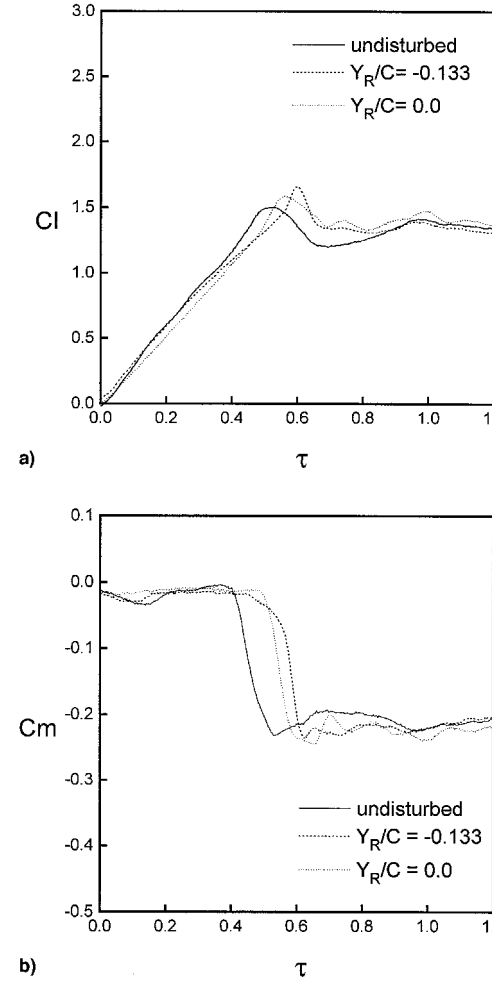

Fig. 8 a) Lift and b) pitching moment curves for disturbed and undisturbed cases at k = 0.01.

Higher Pitch Rates

The influence of freestream disturbances on the upper-surface pressures near the leading edge at higher pitch rates $k = 0.02$ and 0.04 are illustrated in Figs. 9 and 10, respectively. These figures, like Fig. 7, show the values of pressure coefficient vs dimensionless time of the peak suction occurring at $x/c = 0.005$, 0.025, 0.075, and 0.0125. It can be seen that an increase in pitch rate tends to enlarge the magnitude of peak suction and delay the occurrence of peak suction to a higher incidence for the pressures presented. The introduction of freestream disturbances at higher pitch rates has a similar effect to the one observed at the lower pitch rate $k = 0.01$. At $k = 0.02$, in comparison with the undisturbed case the peak suction pressure at the leading edge, ($x/c = 0.005$) is increased by 1.2 and 2.4 in $-C_p$ with a phase delay of 2.6 and 3.8 deg for $Y_R/c = 0$ and -0.133, respectively. For $k = 0.04$, the peak suction at the leading edge is increased by 1.3 and 2.4 in $-C_p$ with a phase delay of 1.6 and 2.8 deg for $Y_R/c = 0$ and -0.133, respectively. In the disturbed circumstances, the absolute magnitude of the peak suction pressure downstream from the leading edge diminishes rapidly with chordwise position. As a result, the influence of the freestream disturbances on the sectional lifts and moments is less significant. This is evident in the comparison of the time histories of Cl and Cm

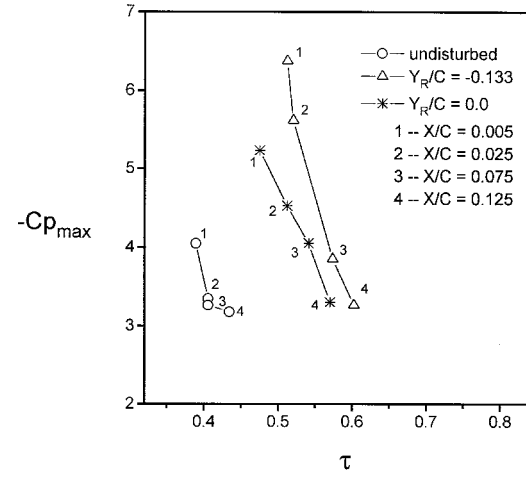

Fig. 9 C_p vs τ of maximum suction for the leading four pressure ports at k = 0.02.

presented in Figs. 11 and 12 for $k = 0.02$ and 0.04, respectively. The maximum lift coefficient apparently has a larger magnitude and occurs at a larger angle of attack for higher pitch rates, and so is the maximum nose-down pitching moment coefficient $-Cm$. For the undisturbed cases, the maximum Cl of 1.85 and 2.65 are reached at $\alpha = 19$ and 30 deg for $k = 0.02$ and 0.04, respectively. On the other hand, the introduction of disturbances yields little effects on magnitudes of maximum Cl and Cm, except for a phase delay. For $k = 0.02$, the phase delay computed from both Cl and Cm time

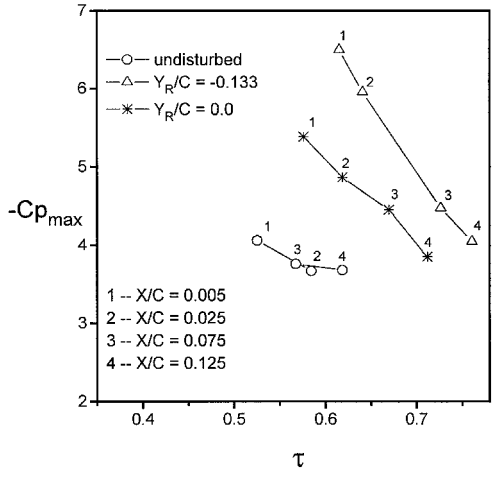

Fig. 10 C_p **vs** τ **of maximum suction for the leading four pressure ports at** k **= 0.04.**

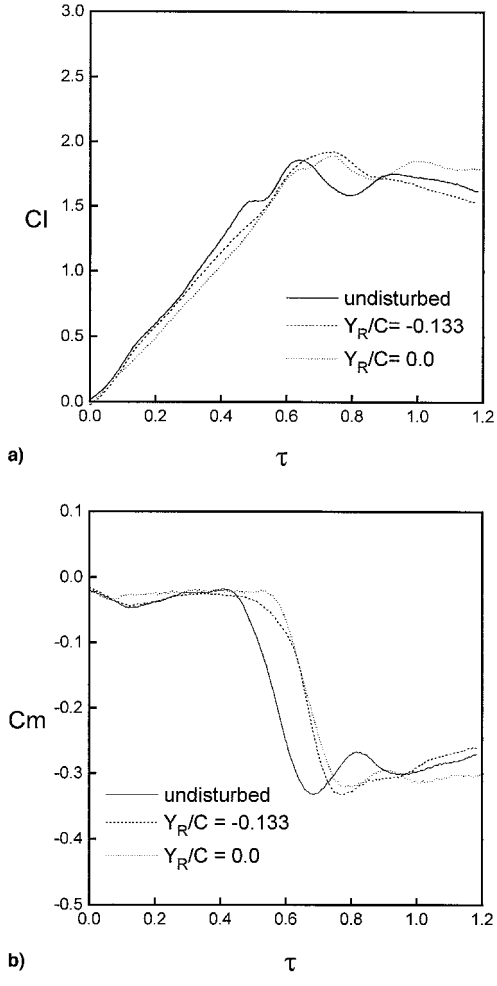

Fig. 11 a) Lift and b) pitching moment curves for disturbed and undisturbed cases at k **= 0.02.**

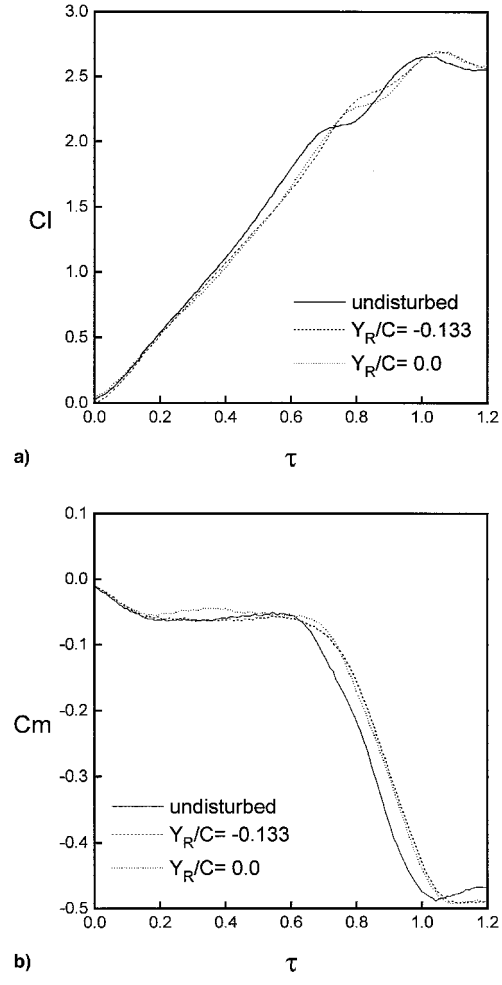

Fig. 12 a) Lift and b) pitching moment curves for disturbed and undisturbed cases at k **= 0.04.**

histories is about 3 deg in incidence. For $k = 0.04$, the phase delay is reduced to about 1.2 deg. At the higher pitch rates $k = 0.02$ and 0.04, shifting the vertical offset between $Y_R/c = 0$ and -0.133 seems to produce a negligible change in Cl and Cm during the dynamic stall process, although it does create some distinct features on the upper-surface pressures near the leading edge.

Some additional insight into the progress of the dynamic stall phenomenon may be obtained by further examination of the lift and moment curves. For $k = 0.02$, the moment curves in Fig. 11b exhibit a sudden dip at around $\tau = 0.6$–0.8. This dip is caused by the presence of a leading-edge-vortex-induced low-pressure cell moving over the airfoil as the vortex convects by the airfoil. The moment curve showing such a dip may be taken as presumptive evidence of the formation, detachment, and convection of the well-organized DSV.[4] In regard to possible leading-edge bubbles mentioned in the Introduction, it may be interesting to note that the lift curves in Figs. 11a and 12a for the undisturbed airfoil actually show plateaus that might indicate bubbles that reattach. These plateaus can be found for all cases in Fig. 12, but for only the undisturbed case for Fig. 11. This may suggest that a turbulent boundary layer alone is not enough to delay the dynamic stall, so that the presence of the rod is more like a vortex generator in terms of energizing the boundary layer.

Conclusions

Pressure measurements have been made on a constant-rate pitching airfoil subjected to a disturbed environment at a chord Reynolds number of 8×10^4. The disturbed environment was produced by employing a thin circular rod at a certain distance upstream of the NACA 0012 airfoil tested. When the upstream rod was placed at nonpositive vertical offset values ($Y_R/c = 0$ and -0.133), for all pitch rates tested, the imposed freestream disturbances were able to increase the absolute magnitude of the peak suction pressure near the leading edge of the airfoil by as much as 50%, compared with the undisturbed case, and the peak suction was reached at a higher angle of attack. The pressure variation as a result of the imposed disturbances was found to be appreciable only in approximately the forward 20% chord from the leading edge. At a more downstream chord, the pressures became less affected except for a

noticeable phase lag. Although the freestream disturbances caused a substantial effect on the upper-surface pressures near the leading edge, the lift and pitching moment coefficients appeared to have a lower disturbance influence. At higher pitch rates ($k = 0.02$ and 0.04), the influence of the imposed freestream disturbances on the sectional lift and pitching moment was less significant than that at a lower pitch rate ($k = 0.01$). The effects of the disturbed environment closely resemble those produced by the increase in the chord Reynolds number.[20,22] The results of pressure measurements reported here indicate that the disturbed environment, having a flow behavior comparable to that at higher Reynolds numbers, tends to promote earlier transition of the unsteady laminar shear layer separating from the leading edge to turbulence, thus effectively reducing the separation region.

Acknowledgment

Financial support for this work from the National Science Council of the Republic of China Contracts NSC 85-2212-E005-021 and NSC 86-2612-E-005-001 is gratefully acknowledged.

References

[1]Carr, L. W., McAlister, K. W., and McCroskey, W. J., "Analysis of the Development of Dynamic Stall Based on Oscillating Airfoil Experiments," NASA TN D-8382, Jan. 1977.

[2]Carr, L. W., "Progress in Analysis and Prediction of Dynamic Stall," *Journal of Aircraft*, Vol. 25, No. 1, 1988, pp. 6–17.

[3]Visbal, M. R., and Shang, J. S., "Investigation of the Flow Structure Around a Rapidly Pitching Airfoil," *AIAA Journal*, Vol. 27, No. 8, 1989, pp. 1044–1051.

[4]Jumper, E. J., Dardis, W. J., III, and Stephen, E. J., "Toward an Unsteady-Flow Airplane," AIAA Paper 88-0752, Jan. 1988.

[5]McCroskey, W. J., Carr, L. W., and McAlister, K. W., "Dynamic Stall Experiments on Oscillating Airfoils," *AIAA Journal*, Vol. 14, No. 1, 1976, pp. 57–63.

[6]McAlister, K. W., and Carr, L. W., "Wind Tunnel Visualization of Dynamic Stall," *Journal of Fluids Engineering*, Vol. 101, Sept. 1979, pp. 376–380.

[7]Francis, M. S., and Keesee, J. E., "Airfoil Dynamic Stall Performance with Large-Amplitude Motion," *AIAA Journal*, Vol. 23, No. 11, 1985, pp. 1653–1659.

[8]Jumper, E. J., Schreck, S. J., and Dimmick, R. L., "Lift-Curve Characteristics for an Airfoil Pitching at Constant Rate," *Journal of Aircraft*, Vol. 24, No. 10, 1987, pp. 680–687.

[9]Strickland, J. H., and Graham, G. M., "Force Coefficients for a NACA-0015 Airfoil Undergoing Constant Pitch Rate Motions," *AIAA Journal*, Vol. 25, No. 4, 1987, pp. 622–624.

[10]Lorber, P. F., and Carta, F. O., "Airfoil Dynamic Stall at Constant Pitch Rate and High Reynolds Number," *Journal of Aircraft*, Vol. 25, No. 6, 1988, pp. 548–556.

[11]Acharya, M., and Metwally, M. H., "Unsteady Pressure Field and Vorticity Production over a Pitching Airfoil," *AIAA Journal*, Vol. 30, No. 2, 1998, pp. 403–411.

[12]Chandrasekhara, M. S., Ahmed, S., and Carr, L. W., "Schlieren Studies of Compressibility Effects on Dynamic Stall of Transiently Pitching Airfoils," *Journal of Aircraft*, Vol. 30, No. 2, 1993, pp. 213–220.

[13]Shih, C., Lourenco, L., and Krothapalli, A., "Investigation of Flow at Leading and Trailing Edges of Pitching-Up Airfoil," *AIAA Journal*, Vol. 33, No. 8, 1994, pp. 1369–1376.

[14]Panda, J., and Zaman, K. B. M. Q., "Experimental Investigation of the Flow Field of an Oscillating Airfoil and Estimation of Lift from Wake Surveys," *Journal of Fluid Mechanics*, Vol. 265, 1994, pp. 65–95.

[15]Tani, I., "Low-Speed Flows Involving Bubble Separations," *Progress in Aeronautical Sciences*, Vol. 5, No. 2, 1964, pp. 70–103.

[16]Mueller, T. J., "The Influence of Laminar Separation and Transition on Low Reynolds Number Airfoil Hysteresis," *Journal of Aircraft*, Vol. 22, No. 9, 1985, pp. 763–770.

[17]Hsiao, F.-B., Liu, C.-F., and Tang, Z., "Aerodynamic Performance and Flow Structure Studies of a Low Reynolds Number Airfoil," *AIAA Journal*, Vol. 27, No. 2, 1989, pp. 129–137.

[18]Mueller, T. J., Pohlen, L. J., Conigliaro, P. E., and Jansen, B. J., Jr., "The Influence of Free-Stream Disturbances on Low Reynolds Number Airfoil Experiments," *Experiments in Fluids*, Vol. 1, No. 1, 1983, pp. 3–14.

[19]O'Meara, M. M., and Mueller, T. J., "Laminar Separation Bubble Characteristics on an Airfoil at Low Reynolds Numbers," *AIAA Journal*, Vol. 25, No. 8, 1987, pp. 1033–1041.

[20]Conger, R. N., and Ramaprian, B. R., "Pressure Measurements on a Pitching Airfoil in a Water Channel," *AIAA Journal*, Vol. 32, No. 1, 1994, pp. 108–115.

[21]Laneville, A., and Vittecoq, P., "Effect of Turbulence on Dynamic Stall," Wind Turbine Aerodynamics Seminar, Sandia National Labs., Albuquerque, NM, March 1985.

[22]Chen, J. M., and Lee, J.-H., "Surface Pressure and Dynamic Characteristics on a Pitching Airfoil," *Journal of Chinese Society of Mechanical Engineers*, Vol. 18, No. 6, 1997, pp. 567–578.

[23]Kiya, M., and Sasaki, K., "Free-Stream Turbulence Effects on a Separation Bubble," *Journal of Wind Engineering and Industrial Aerodynamics*, Vol. 14, 1983, pp. 375–386.

[24]Batill, S. M., and Nebres, J. V., "Application of Digital Filtering Techniques to Unsteady Pressure Measurements," AIAA Paper 91-0061, Jan. 1991.

[25]Rennie, R. M., and Jumper, E. J., "Experimental Measurements of Dynamic Control Surface Effectiveness," *Journal of Aircraft*, Vol. 33, No. 5, 1996, pp. 880–887.

[26]Rae, W. H., Jr., and Pope, A., *Low-Speed Wind Tunnel Testing*, 2nd ed., Wiley, New York, 1984, pp. 344–444.

[27]Kuethe, A. M., and Chow, C. Y., *Foundations of Aerodynamics: Bases of Aerodynamic Design*, 4th ed., Wiley, New York, 1986, pp. 138–177.

[28]Jumper, E. J., and Hugo, R. J., "Loading Characteristics of Finite Wings Undergoing Rapid Unsteady Motions: A Theoretical Treatment," *Journal of Aircraft*, Vol. 31, No. 3, 1994, pp. 495–502.

[29]Bloor, M. S., "The Transition to Turbulence in the Wake of a Circular Cylinder," *Journal of Fluid Mechanics*, Vol. 19, No. 2, 1963, pp. 290–304.

[30]Michelsen, W. D., and Muller, T. J., "Low Reynolds Number Airfoil Performance Subjected to Wake Interference from an Upstream Airfoil," AIAA Paper 87-2351, Aug. 1987.